



Selective Windows for Sudan

Manahil. H. balal¹, M. O. Sid-Ahmed² and Ahmed. H.Elfaki³

¹Department of Physics, Faculty of Education, University of Gadarif , Gadarif, Sudan

²Department of Physics, College of Science, Omdurman Ahlia University, Omdurman, Sudan

³Department of Physics, College of Science, Sudan University of Science and Technology, Khartoum, Sudan

Corresponding Author: manahbelal@gmail.com

Received: May 2017

Accepted: October 2017

Abstract

Buildings in Sudan espouser amount of heat gain through windows, this affects the thermal comfort of buildings' occupants. The windows are needed to transmit natural light, nor heat. Rigorous coupled-wave analysis (RCWA) has been used as a simple filter to transmits most of the visible light and reflects most of the infrared radiation. The filter has been prepared by using magnetron sputtering technique at the University of Witwatersrand(Wits), South Africa. There has been very good agreement between the simulation results and the experimental results.

Keywords: smart windows, magnetron sputtering, hot climates, electrochromic windows, thermochromic windows.

© 2017 Sudan University of Science and Technology, All rights reserved

المستخلص

تتعرض المباني في السودان الى كمية كبيرة من الطاقة الحرارية من خلال النوافذ، مما يؤثر على راحة السكان. ومن المفترض ان تسمح النوافذ بمرور الضوء لكن ليس الحرارة وقد تم استخدام برن ج (rigorous coupled-wave analysis (RCWA) لتصميم نافذة انتقائية بسيطة تسمح بمرور الضوء المرئي وتعكس معظم الأشعة تحت الحمراء. تم تصنيع النافذة بتقنية magnetron sputtering technique في كلية العلوم جامعة (Wits) في جنوب افريقيا. وقد كان هناك توافق بين نتائج المحاكاة والنتائج التجريبية.

Introduction

In the north of Sudan, the climate is desert, and in particular the northernmost area, near the border with Egypt, is one of the driest and sunniest in the world. Winter temperatures are pleasantly mild by day and cool at night, even cold at times, especially in the far north, where it can

occasionally drop to around freezing. The rest of the year is rather hot, with highs around 40°C from May to October, but with records of 50-52 °C. The wind can raise sandstorms at any time of the year⁽¹⁾. The average temperature at Wadi Halfa is shown in Table.1.

Table1. Average temperatures at Wadi Halfa

WadiHalfa	Jan	Feb	Mar	Apr	May	Jun	Jul	Aug	Sep	Oct	Nov	Dec
Min(°C)	7	8	12	16	21	23	23	23	22	19	14	9
Max(°C)	23	26	31	36	40	41	41	40	38	36	30	25

Khartoum is located at 400 meters above sea level, where the White Nile and the Blue Nile meet. With an average annual temperature of 30 °C, Khartoum is one of the hottest capitals in the world. In winter, reaches more than 31 °C even in January,

but sometimes it can get cold at night, in fact the cold record is only 1 °C; in spring the temperatures increase rapidly, so that they reach 40 °C already in April, Table.2. In April and May sometimes the temperature have reached 47 °C.

Table2. Average temperatures at Khartoum

Khartoum	Jan	Feb	Mar	Apr	May	Jun	Jul	Aug	Sep	Oct	Nov	Dec
Min(°C)	16	17	20	24	27	28	26	26	26	26	21	17
Max(°C)	31	33	37	40	42	41	39	38	39	39	35	32

In July and August, under the influence of the monsoon, which brings a bit of rain, the temperature decreases slightly, but it remains very high, around (38-39) °C, and then between October and November, at the end of the monsoon, it increases slightly again, rising to (39-40) °C. This high temperature requires development of suitable architecture for the buildings and finding means of reducing the heat through the windows of houses and vehicles.

The solar Energy in Sudan is available during the years. The average daily solar irradiation is 5.8 – 7.2 kWh/m². The maximum, 7.2 kWh/m², is in the north west

of the country, while the minimum, 5.8 kWh/m², is in the south west⁽²⁾.

The total generated electricity in Sudan is about 11.665 GWh. The house holdsector consumes about 52% of the total energy consumption; Fig.1. The consumption of electricity per capita is about 285 kWh/year.

The consumption of electricity in the household sector for lighting and cooling is about 3.5x 10⁶ M Wh per year. This can be greatly reduced by using spectrally selective windows, in the houses, which reflect the heat and transmit the light.

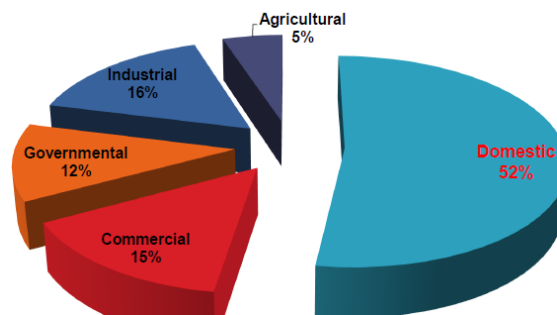


Figure.1 Energy consumption in Sudan[2]

Smart Windows

Smart glass is a glazing whose light transmission properties are altered when voltage, light or heat is applied. Generally, the glass changes from translucent to transparent, changing from blocking some (or all) wavelengths of light to letting light pass through. Smart glass technologies include electrochromic and thermochromic.

Electrochromic devices change light transmission properties in response to voltage and thus allow control over the amount of light and heat passing through. It changes between a colored, translucent state (usually blue) and a transparent state. A burst of electricity is required for changing its opacity, but once the change has been achieved, no electricity is needed for maintaining the particular shade which has been reached. Electrochromic glass provides visibility even in the darkened state and thus preserves visible contact with the outside environment⁽³⁾. The transition from clear to opaque takes 3-5 minutes, for a small window⁽⁴⁾. Hong and Chen⁽⁵⁾ used nano-Prussian blue analogue/PEDOT/PSS:composites for a $10 \times 10 \text{ cm}^2$ WO_3 electrochromic window. A maximum transmittance modulation of 61.6% at a voltage of 1.6 V was obtained. Kim and Taya⁽⁶⁾ used V_2O_5 and poly(3,3-dimethyl-3,4-dihydro-2H-thieno [3,4-b][1,4]dioxepine) coatings. The window demonstrated electrochemical stability after over 150,000 cyclic switches and that the response time for a $25 \times 25 \text{ mm}^2$ window was 5 seconds for coloration and 4 seconds for bleaching. Similarly, Kim et al⁽⁷⁾ obtained high electrometric contrast and optical cyclic stability, when they used electrochromic polymers on lenses containing 9H-carbazole-9-ethanol moieties. Fernandes et al⁽⁸⁾ used glass/ITO/ WO_3 /electrolyte/ITO/glass layered configuration. That resulted on visible average transmittance variation and optical density change of 41.6% and 0.39, respectively. Hee et al⁽⁹⁾ concluded that

electrochromic windows are more suitable for applications in residential areas in cold climate regions. Brooke et al⁽¹⁰⁾ investigated the effect of oxidant on the performance of conductive polymer films. They concluded that the oxidant $\text{Fe}(\text{Tos})_3$ produced superior device performance with respect to optical switching, switch speed and optical relaxation. Kim et al⁽¹¹⁾ prepared transparent conductive ZnIn SnO-Ag- ZnIn SnO multilayer films for polymer dispersed liquid-crystal based smart windows. They obtained a lower operating voltage and a higher cutoff rate of infrared light, compared to ITO or ZITO-based smart windows. Khandelwal et al⁽¹²⁾ fabricated electrically switchable broadband infrared reflectors using polymer stabilized cholesteric liquid crystals. They predicted that their reflector can save more than 12% of energy compared to double glazing window and 9.3% compared to static infrared reflector. One of the drawbacks of electrochromic windows is their need for external biases to operate. Wang et al⁽¹³⁾ introduced a self-powered window. Aluminum was used to reduce Prussian blue to Prussian white in potassium chloride electrolyte. For self-recovering of the device to the blue appearance, the aluminum and Prussian blue electrodes could be disconnected. Lim et al⁽¹⁴⁾ studied the performance of tungsten-oxide-based electrochromic window. The results showed that the transmittance of visible light varied from 64% in the clear state to very low values in the colored state. They also concluded that there is little additional benefit from placing low emissivity coating on the electrochromic window. Ranjit A. Patil et al⁽¹⁵⁾ used pure 1D brookite TiO_2 nanoneedles grown on a conducting indium tin oxide thin film coated glass substrate. The electrochromic characteristics include stable and reversible coloration-bleaching cycles, and high-value diffusion coefficient ($1.56 \times 10^{-11} \text{ cm}^2/\text{s}$), high reversibility (~99%), great coloration efficiency ($226 \text{ cm}^2/\text{C}$), high optical transmittance difference (67%), large optical

density(0.85), and fast coloration and bleaching times (13.10 and 5.14s) at a wavelength of 600nm.

Thermochromic windows switch from a clear state in low temperature to a diffuse reflective state in high temperature⁽¹⁶⁾. The results of Linshuang Long et al⁽¹⁷⁾ showed that the adoption of the VO₂ double-glazed window reduced the cumulative cooling energy consumption by approximately 11.1% compared with an ordinary double-glazed window. Zheng et al⁽¹⁸⁾ designed TiO₂ (R)/VO₂ (M)/TiO₂ (A) multilayer film to work as a smart window with antifogging and self-cleaning functions. Koo et al⁽¹⁹⁾ fabricated CeO₂ – VO₂ bi layer to improve the optical properties of VO₂ window. The CeO₂ was employed as an antireflection layer of the VO₂ film. Kamalisarvestani et al⁽²⁰⁾ studied the spectral selective properties of thermochromic windows and the effect of doping of VO₂ coatings with different dopants.

VO₂ could be the most promising thermochromic material, but its drawback is the preparation cost and the stability. Polymer-assisted deposition preparation method could be more suitable for practical applications than gas-phased methods⁽²¹⁾. Another promising technology is a multilayer thin film structure, consisting of dielectric and metal layers⁽²²⁾. Batista et al⁽²³⁾ concluded that tungsten was the most

effective dopant on the reduction of the semiconductor-metal transition temperature of VO₂. More energy could be saved by using VO₂ double window. Long and Ye⁽²⁴⁾ suggested that an appropriate phase transition temperature is needed to make the VO₂ remains principally in its metallic state with low solar transmittance for summer application and in its semiconductor state with high solar transmittance for winter application. Zhou et al⁽²⁵⁾ combined a VO₂ thermochromic window with solar cells operated by the scattered radiation from the window. However, the efficiency of the cell was too low to justify the additional cost. Wei Feng et al⁽²⁶⁾ studied the effect of Gasochromic (GC) smart window on the energy consumption for a commercial office building. The results showed that GC smart windows can decrease the annual consumption of HVAC loads by 25–35% in all cities.

Both electrochromic and thermochromic windows suffer from high cost, low transmission of visible light and slow response time. In tropical regions, the ideal window is the one which transmits all the visible light to reduce the lighting load, and reflects all the infrared radiation to reduce the cooling load. In this paper we develop a relatively simple, efficient and cheap glazing. The proposed structure is for hot climates. It consists of alternating layers of Si/SiO₂ Figure.2. The performance of the glazing was studied by using rigorous coupled-wave analysis (RCWA) method.

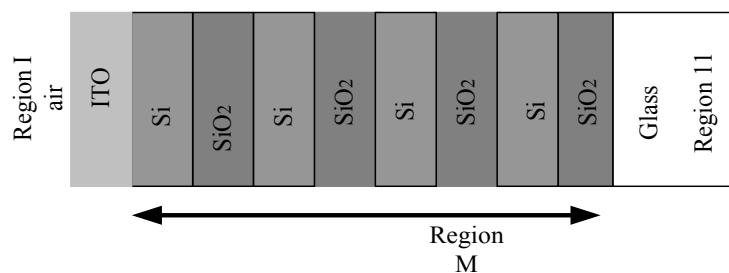


Figure.2 The proposed selective filter

Optimization of the Thickness of The Layers

Rigorous coupled-wave analysis (RCWA) is used in this study to calculate the radiative properties (reflectance and transmittance) of the periodically multilayer surfaces. RCWA is formulated in the 1980 s by Moharam and Gaylord. It is used for analyzing the diffraction of electromagnetic waves by periodic gratings (27). It analyzes the general diffraction problem by solving Maxwell's equations accurately in each of the three regions (input, multilayer, and output), based on Fourier expansion (28). In RCWA, diffraction efficiency for each diffraction order is calculated with incident wave properties regards less of feature size, structural profiles, and dielectric function of the materials.

Results of Simulation

Optimization of Si Thickness

The glazing consists of ITO layer deposited on one-dimensional (1D) four pairs of Si/SiO₂ layers on top of a 1mm-glass sheet, Figure.2. The geometric parameters used to illustrate the

wavelength selective filter are the thicknesses of the layers.

The wavelength-dependent dielectric optical constants of ITO, silicon and silicon dioxide were obtained from Ref (29). The thickness of ITO was 0.1 μm and that of Si was $d_1=0.1, 0.15$ and $0.2\mu\text{m}$. The thickness of SiO₂ was fixed at $d_2=0.4\mu\text{m}$. The normal reflectance and transmittance for the proposed selective filter were calculated numerically by using RCWA method in the wavelength range from 0.3 μm to 3 μm. The normal reflectance and transmittance of the glazing, at normal incidence TM waves, is shown in Figure.3. The results show that the optimum thickness of the Si is 0.15 μm. It gives low reflectance (less than 30%) for wavelengths less than 0.8 μm and reflectance of nearly unity for higher wave length values. This would transmit most of the visible light (to reduce the lighting load) and reflects nearly all the infrared (to reduce the cooling load).

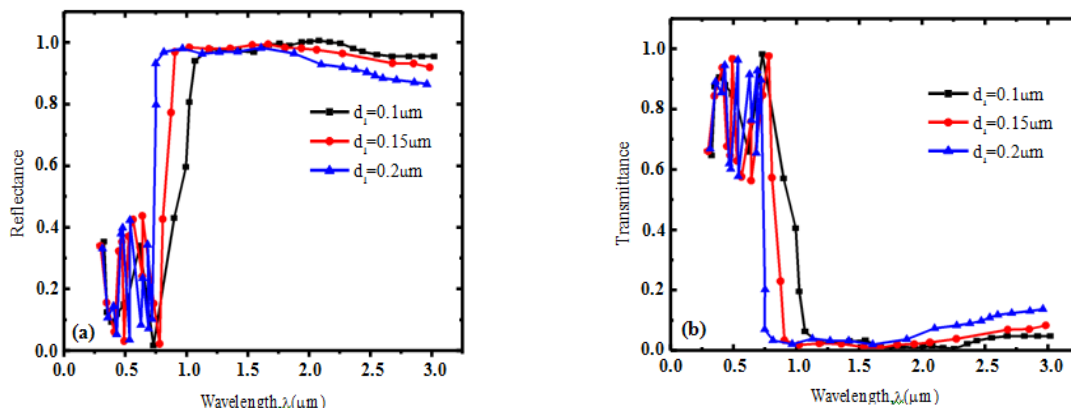


Figure.3. The proposed selective filter for wave with different d_1 thicknesses. (a) shows the reflectance and (b) the transmittance.

Optimization of SiO₂ Thickness

Figure.4 shows the normal reflectance and transmittance of the glazing for normal incidence TM waves. The thickness of Si was taken to be 0.15 μm, while that of

SiO₂ was changed, $d_2= (0.2, 0.3$ and $0.4)\mu\text{m}$. The results show that the optimum thickness for SiO₂ is 0.4 μm.

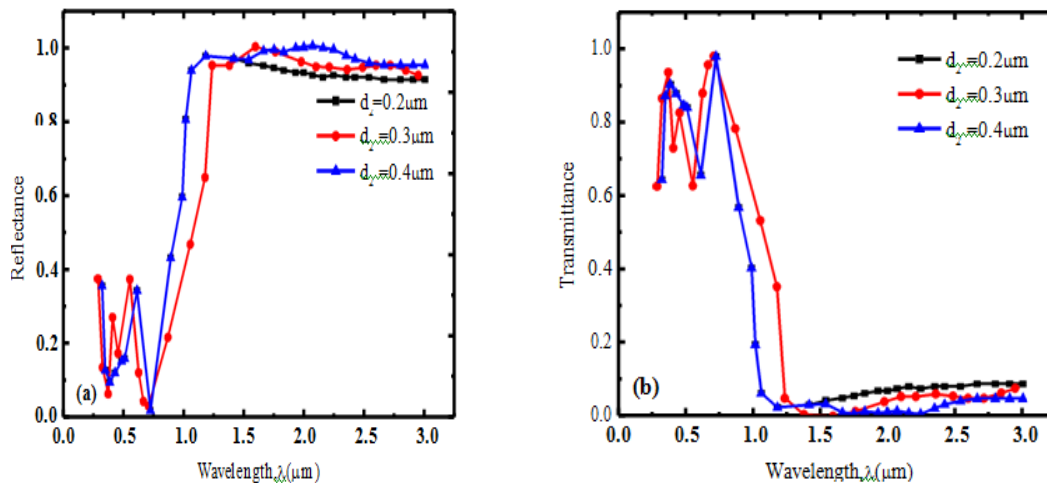


Figure.4. the glazing with different SiO₂ thicknesses. (a) shows the reflectance and (b) the transmittance

Instrumentation

Describe in this section the instrumentations used for preparing and measuring the properties performance of the filter. The fabrication was by magnetron sputtering technique. The spectrophotometer was used to measure the reflection and transmission of the radiation.

Magnetron Sputtering Subsystem

The system employs sputter deposition which is often commonly referred to as sputtering. Sputtering is a process whereby atoms of a solid target are ejected (or vaporized) due to the 'momentum transfer from an atomic-sized energetic bombarding particle' impinging on the target surface⁽³⁰⁾. These vaporized particles will then condense upon and coat a substrate material. Typically sputtering is performed using gaseous ions from plasma that are then accelerated and directed toward the target (although it is also possible to use an ion gun in place of generating ions by producing plasma). The system uses plasma produced and controlled by magnetron guns. The magnetron sputtering system provides the solid material to be deposited onto the substrate. Sputtering is the physical vaporization of atoms from a target surface to form a thin film onto a substrate by momentum transfer from

bombarding energetic atomic sized particles. These atoms, ejected from a target, have a wide energy distribution. The vacuum chamber of the physical vapor deposition (PVD) is filled with an inert gas such as argon. The advantages of the magnetron sputtering that it uses magnets to increase the percentage of electrons that take part in ionization events, increases the probability of electrons striking argon, increases electron path length, lowers voltage needed to strike plasma, controls uniformity, reduces wafer heating from electron bombardment and increases deposition rate. There are large varieties of techniques for sputter deposition of the materials such as radio frequency (RF) magnetron sputtering, DC magnetron sputtering, pulsed DC magnetron sputtering, ion and plasma beam sputtering⁽³⁰⁾.

Magnetron Sputtering Guns and Target Configuration

The geometry of the sputter deposition system determines many of the factors that affect the properties of the deposited film and the throughput of the system⁽³⁰⁾. Yet there are also more obvious practical design considerations that are determined by the use of a sputter system. Sputtering allows for the overall system to be much more compact and for the target to substrate distance to be smaller. This is because the

sputter sources operate at lower temperatures and cause less heating than would be found in a vaporization based system⁽³⁰⁾. A smaller volume system will have less space to be evacuated and less surface area for contaminants to adsorb onto. This decreases pump down time and makes it easier to maintain high system purity. A magnetron sputter system also provides for co-deposition of films by using multiple magnetron guns spaced closely together. The three magnetron guns used in

this work are shown in Figure 5. The arrangement approximates a cylindrical target and allows a more uniform distribution of incident flux on an object placed at the center or focus of the slightly angled magnetron guns. The vertical position of the sample can be adjusted so that it is at the focus of the three guns. Each magnetron has its own shutter so that it can be protected from sputtered material when not in use.

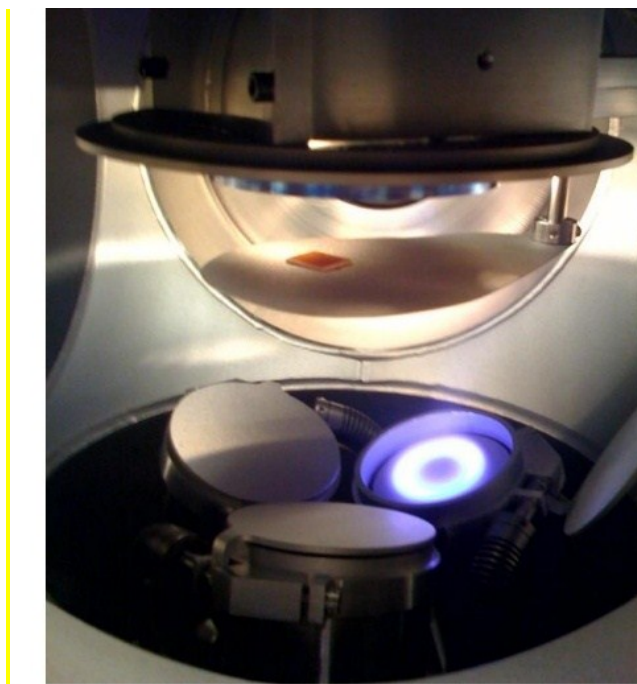


Figure 5. Active argon plasma and substrate heater as seen from main viewport

Sputter Targets

The targets themselves are simply 3-inch (diameter) disks of the chosen material. To prevent overheating (and melting) of the targets the magnetron guns are actively cooled. To increase heat removal, the targets are typically screwed or bonded to a copper backing plate. The uranium and cerium targets are both brittle causing the threads to break off thus detaching the targets from the copper plates unless bonded with thermal compound. Heating of the targets can cause them to expand slightly, but the greatest

change in the target shape is from sputtering. “In planar magnetron sputtering the target develops a ‘racetrack’ depression on the surface. This changing geometry can affect the deposition rate, vapor flux distribution, and other deposition parameters such as the amount of reactive gas needed for reactive deposition in reactive sputter deposition” . Typically, only a fraction of the sputter target (usually “10 to 30” percent) is used as the “racetrack erosion” determines the overall lifetime of the target⁽³⁰⁾. This time can be

increased by removing the target and melting it so that the surface becomes uniform once more. However, this can introduce impurities into the target and it is usually simpler and more cost effective to buy a new target.

Gas Distribution System

The gas distribution system consists of a (vacuum) chamber, a pump for evacuating (or reducing the pressure of) the chamber, a means of measuring and introducing gas into the system, and a means of measuring and controlling the overall pressure in the chamber. The basic design decisions involved in developing the gas distribution system are explained below.

Pumping System Design

The level of cleanliness desired for a particular process determines the vacuum range at which a system is required to operate. By extension it determines the type of vacuum pump or pumps required to achieve and maintain the vacuum. The lower the pressure (or higher the vacuum) required the greater the price of system components and the higher the degree of system cleaning and preparation required.

Measurement and Pressure Control using the Gate Valve

Several types of pressure sensors are used in this system design. These sensors function based on different methods which determine the range of operability.

Gas Supplies, Mass Flow Controllers, and the Gas Injection Manifold

The reactive gas and the working gas supplies used are “five nines” and “six nines” pure, respectively (i.e. 99.999% O₂ and 99.9999% Ar). Each gas supply used a dual-vane high-purity all stainless steel regulator valve (specific to that gas/bottle connection). Use of dual-vane regulators, as opposed to single vane regulators, allows the gas supplied to remain at a continuous (non-fluctuating) pressure as long as there is gas available in the tank. The regulators have stainless steel VCR connections and are connected to lock-in integral VCR valves (which were cleaned by the manufacturer to clean room standards). The secondary valves then connect to custom-ordered ¼ in. stainless steel piping with VCR connections that were bent into the desired shaped using a pipe bender. These metal gas lines transport the gases to their respective Mass Flow Controllers (MFCs). The tanks and associated valves and piping are shown in Figure 6. Note that for safety purposes, the O₂ line also has a flash suppressor so that if flammable gas were somehow introduced into the line and ignited it could not back flow into the O₂ tank. Additionally, the regulators only allow pressures of up to 30 to 40 psi. This is intentional so that the gas lines cannot become over-pressurized⁽³⁰⁾.



Figure 6: Gas tanks (left to right: O₂, Ar, “low” purity Ar, and Air) and associated hardware

filter consists of ITO layer deposited on four pairs of Si/ SiO₂ layers on top of a 1mm-glass sheet.

The magnetron sputtering system, Figure.7, was used to deposit a thin film from sputtering targets onto substrate.

The silicon (Si) and silicon dioxide (SiO₂) were used as sputtering targets. The sputtering power and pressure were kept at 100 W and 140W for silicon and silicon dioxide, respectively, and operation pressure at 5.7×10^{-3} Pa. The base vacuum level was 5.3×10^{-3} Pa. The Argon gas flow rate was kept at 20 (standard cubic centimeters per minute) and controlled by a mass flow meter. A single Si layer was deposited on quartz substrate for 5min, and a single SiO₂ layer was deposited on it for 20min. The thicknesses of ITO, Si and SiO₂ were 0.1µm, 0.15 and 0.4 µm, respectively.

Maintenance and Cleaning

Regular maintenance and cleaning will need to be performed on the magnetron sputtering system. For practical and convenience purposes, it was designed to minimize down times associated with these tasks.

Sample Storage

Although not technically part of the system, there are several storage options available for completed film samples. The storage methods are designed to mitigate the post-deposition contamination of the films. Examples of post-deposition include oxidation of the completed film or the adsorption of contaminants such as hydrocarbons. (Water vapor accumulation can also be detrimental to films). While inside the system, post-deposition contamination will remain unlikely.

Experimental Work

The preparation and measurements of the filter were performed at the laboratories of the Faculty of Science, University of Witwatersrand (Wits), South Africa. The



Figure.7 The sputter deposition system WARNING (Wits) of Technology Lab.

Experimental Result

The measurement of the reflectance and transmittance are shown in Figure.6. The results show that the filter transmits about

78% of the visible light and reflects nearly all the infrared. The results are almost typical to that obtained by the simulation.

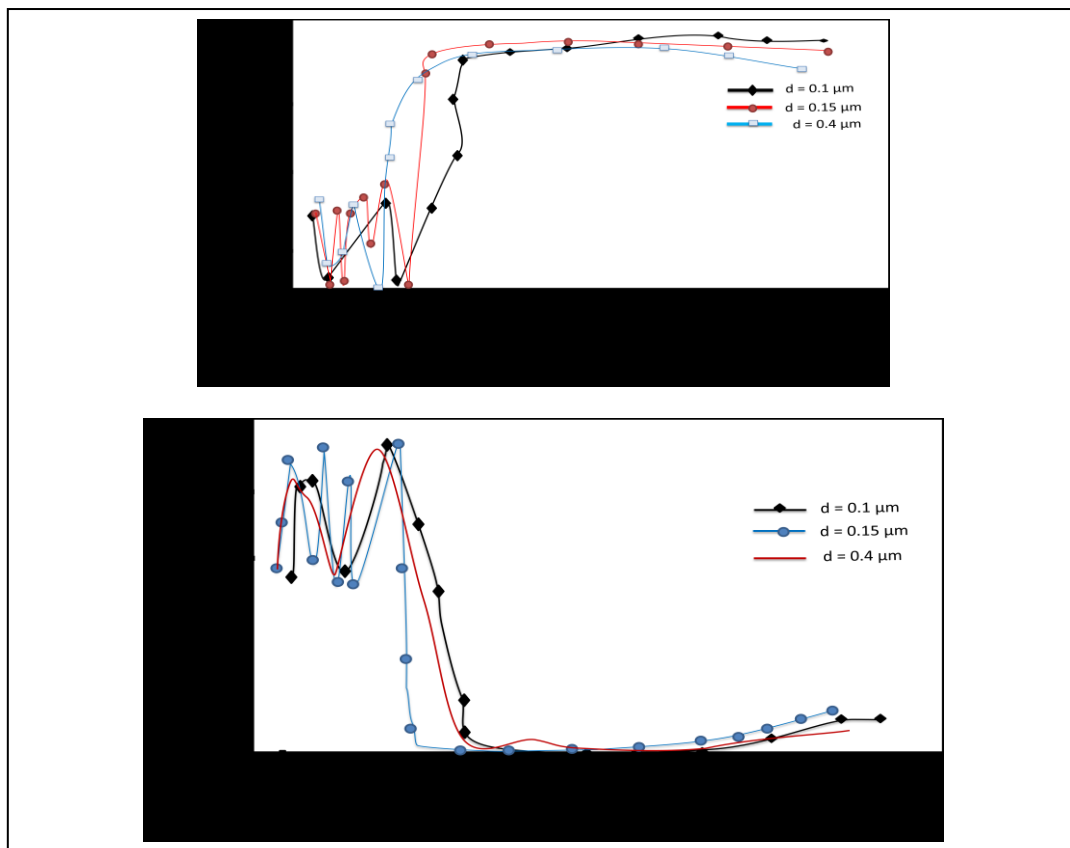


Figure.7. Reflectance and transmittance of the filter.

Conclusion

In summary, we have used rigorous coupled-wave analysis (RCWA) to design a relatively simple and efficient glazing for hot climates. The glazing consisted of ITO and four periodic pairs of Si/SiO₂, deposited on a glass sheet.

RCWA was used to calculate the reflectance and transmittance of the different thicknesses of the layers. The preparation of the filter and the testing were performed at the laboratories of the Faculty of Science, University of Witwatersrand, South Africa. The optimum thicknesses of ITO, Si and SiO₂ were found to be (in both simulation and experimental work) 0.1 μm, 0.15 μm and 0.4 μm, respectively. The glazing transmitted 78% of the visible light and reflected almost all the infrared radiation from the sun. The optical properties of the glazing hardly depended on the angle of incidence of solar radiation. This makes it ideal for all hours of the day. During the night, in winter, I could

act as an insulator to reflect the heat back inside the room. It satisfies the conditions for comfort in both the hot days of summer and the cold nights of winter.

References

1. Info@climatestotravel.com
2. Ministry of Water Resources, Irrigation and Electricity.
3. Lee, E.S., S.E. Selkowitz, R.D. Clear, D.L. DiBartolomeo, J.H. Klems, L.L. Fernandes, G.J. Ward, V. Inkarojrit, M. Yazdani. 2006. *Advancement of Electrochromic Windows*. California Energy Commission, PIER. Publication number CEC-500-2006-052.
4. S. E. Rudolph, J. Dieckmann, J. Brodrick, *Ashrae Journal* (2009) 104-107.
5. S. Hong and L. Chen, *Solar Energy Materials & Solar Cells* 104 (2012) 64-74.

6. S. Kim and M. Taya, *Solar Energy Materials & Solar Cells* 107 (2012) 225-229.
7. S. Kim, X. Kong and M. Taya, *Solar Energy Materials & Solar Cells* 117 (2013) 183-188.
8. M. Fernandes, V. T. Freitas, S. Pereira, E. Fortunato, R.A.S. Ferreira, L.D. Carlos, R. Rego, V. Bermudez, *Solar Energy Materials & Solar Cells* 123 (2014) 203-210.
9. W. J.Hee, M.A. Alghoul, B. Bakhtyar, E. OmKalthum, M. A. Shameri, M. S. Alrubaih, K. Sopian, *Renewable and Sustainable Energy Reviews* 42 (2015) 323-343.
10. R. Brooke, M. Fabretto, N. Vucaj, K. Zuber, E. Switalsaka, L. Reeks, P. Murfy and D. Evans, *Smart Mater. Struct.* 24 (2015) 035016.
11. E. Kim, I. Choi, J. Oh, Y. Kim, J. Lee, Y. Choi, J. Cho, Y. Kim and G. HEO, *Japanese Journal of Applied Physics* 53 (2014) 095505.
12. H. Khandelwal, R. Loonen, J. Hensen, M. Debije and A. Schenning, *Scientific Reports* 5 (2015) 11773.
13. J. Wang, L. Zhang, L. Yu, Z. Jiao, H. Xie, X. W. Lou, X. W. Sun, *Nature Communications* 5921 (2014).
14. S. H. N. Lim, J. Isidorsson, L. Sun, B. L. Kwak and A. Anders, *Solar Energy Materials & Solar Cells* 108 (2013) 129-135.
15. Ranjit A.Patil, RupeshS.Devan, YungLiou and Yuan-RonMa, *Solar Energy Materials & Solar Cells* 147 (2016) 240-245.
16. L. Long, H. Ye, H. Zhang and Y. Gao, *Solar Energy* 120 (2015) 55-64.
17. Linshuang Long, Hong Ye, Haitao Zhang and Yanfeng Gao, *Solar Energy Materials & Solar Cells* 120 (2015) 55-64.
18. Jianyun Zheng, Shanhu Bao and Ping Jin *Nano Energy* 11 · January (2015).
19. H. Koo, D. Shen, S. Bae, K. Ko, S. Chang and C. Park, *Journal of Material Engineering and Performance* 23 (2014) 402-407.
20. M. Kamalifarvestani, R. Saidur, S. Mekhilef, F.S. Javadi, *Renewable and Sustainable Energy Reviews* 26 (2013) 353-364.
21. Y. Mouedden et al. *Proceeding of 9th International Conference(HONET)* (2012) 83-86 Istanbul, Turkey.
22. S. G. Babiker et al/ *WSEAS Transactions on Applied and Theoretical Mechanics* 9 (2014)97-103.
23. C. Batista, R. Ribero and V. Teixeira, *Nanoscale Research Letters* (2011) 6:301.
24. Linshuang Long and Hong Ye, *Solar Energy Materials & Solar Cells* 107 (2014) 236-244.
25. J.Zhou, Y. Gao, Z. Zhang, H. Luo, C. Cao, Z. Chen, L. Dai and X. Liu, www.nature.com/scietificreports 3:3029 (2013).
26. WeiFeng, LipingZou, GuohuaGao, GuangmingWu, JunShen and WenLi, *Solar Energy Materials & Solar Cells* 144 (2016) 316-323.
27. M.G. Moharam, and K.T. Gaylord, "Rigorous coupled-wave analysis of planar-grating diffraction," *Opt. Express*, 71 (1981)811-818.
28. S. Peng and M.G. Morris, "Efficient implementation of rigorous coupled-wave analysis for surface-relief gratings," *Opt. Express*, 12 (1995)1087-1096.

29. D.E. Palik, "Handbook of Optical Constants of Solids," Academic Press, San Diego, CA, (1985).

30. Mattox, D. (1998). *Handbook of Physical Vapor Deposition (PVD)*

Processing: Film Formation, Adhesion, Surface Preparation and Contamination Control. Park Ridge, New Jersey: Noyes Publications.